Supplementary Material, Part 1

We present in the first section of this supplement two figures that support the main text and are referenced in the discussion the Government Flats Complex Fire (Sections 3.1 and 3.2).

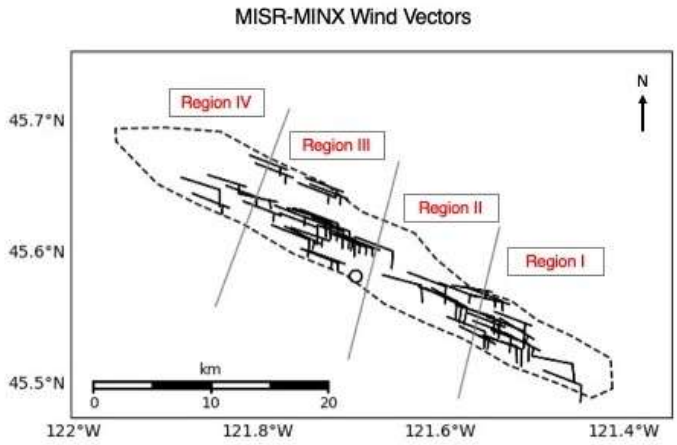

Figure S1. Wind trajectories retrieved from the MISR-MINX software tool (in units of knots) for the Government Flats Complex Fire. Half-barbs indicate 5 knots, full barbs are 10 knots. The grey lines represent the regional boundaries within the plume (See Fig. 1a). Empty circles are points where the retrieved wind speed was zero.

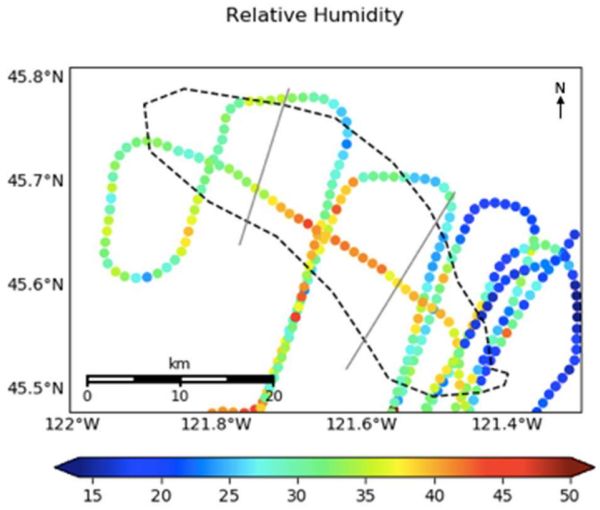

Figure S2. Percent relative humidity observed from the BBOP G-1 aircraft for the Government Flats Complex Fire.

Supplementary Material, Part 2

We present in the second section of this supplement detailed descriptions of the *in situ* and spacecraft observations collected for the Government Flats Complex Fire, by region. (This elaborates on Sections 3.1 and 3.2 in the main text.)

I. Aircraft *in situ* Observations of the Government Flats Complex Fire

As expected, the *in situ* observations indicate the highest CO and aerosol concentrations near the source, decreasing downwind. Virtually all points outside the plume boundaries contain fewer than 2,000 particles/cm^3, as measured by the PCASP/CAS (Figure 1d), and less than 0.15 ppm of CO (Figure 1c). The sections below use the regional statistical data from Table 4 in conjunction with the lat/lon plots in Figures 2 and 3 to characterize in detail each plume region, with emphasis on the *differences* from one region to the next. This allows us to both quantify large-scale patterns as well as to visualize small-scale changes, and to account for any differences in sample size. Note that discussion of large aerosols has been omitted, as their fractions are negligible, although Figure 3 and Table 4 contain the available information on these particles. Also note that discussion of differences in $r_{e(BC)}$ are mostly omitted, as all are likely within the uncertainty of the SP2; however, we retain the regional mean values in Table 4.

Region I

The near-source region contains, on average, the freshest (-log[NO_x/NO_y] ~0.2) and darkest (SSA ~0.7) particles, as well as the highest mean BC mass and $r_{e(BC)}$ (over 16,000 #/cm^3 and 0.070 μm, respectively) (Figure 2). Overall, the region is dominated by small and medium aerosols, with mean fractions of ~57% and ~31%, respectively (Table 4). Apart from the BC particles we know to be present from SP2 measurements, very small aerosols are almost absent throughout most of the region, except for two extreme outlier pixels that contain fractions higher than 60% and therefore inflate the mean to ~13% (the median is ~3.8%, a value that is more likely representative).

Region II

Compared to upwind, the near-downwind region contains considerably more oxidized, brighter particles, with mean -log[NO_x/NO_y] and SSA of ~0.53 and ~0.77, respectively (Table 4 and Figure 2; as has been mentioned, filter-based SSA measurements tend to bias low under heavy aerosol burdens, so the actual SSA values may be somewhat higher). The mean absolute BC mass concentration decreases nearly two-fold to ~8,600 #/cm^3, although it is higher within the central portion of this region compared to the plume edges (Figure 2c), where there is entrainment of fresh air. The mean CO-normalized BC mass concentration also decreases significantly, although the median increases. In the central, along-plume transect, there are dramatic increases in both the CO-normalized absorption attributed to BrC (over 25% on average) and the CO-normalized ultraviolet (UV) scattering (38% on average) (Table 4). The CO-normalized CCN_{15} and aerosol concentrations both increase by more than 80% from Region I. Aerosol size decreases compared to upwind, with increasing fractions of small and very small particles along with a decreasing fraction of medium aerosols. However, this change is only seen along the plume boundaries (Figure 3), where the fraction of very small particles is ~20-50% higher than the rest of the region, and similarly, medium aerosol fractions are 20-50% lower. Overall, the central, major portion of the plume appears to show no great differences in the partitioning of aerosol size categories compared to upwind, but SSA, aerosol oxidation, BrC absorption, UV scattering, and normalized CCN_{15} concentration increase measurably, and BC mass concentration decreases.

Region III

The mid-downwind region displays further oxidation and SSA enhancement (means of ~0.79 and ~0.78, respectively). Unsurprisingly, this is accompanied by a plume minimum in mean BC mass concentration. Mean CO-normalized BC mass concentration decreases again from Region II, while median concentration slightly increases. CO-normalized UV scattering slightly increases compared to Region II, whereas the mean and median CO-normalized BrC absorption slightly decrease and slightly increase, respectively (and the mean still remains much higher than that of Region I). Furthermore, both the normalized CCN_{15} and normalized total aerosol count peak in this region (Figure 2). There is also a ~10% regional-mean increase in the fraction of very small aerosols, accompanied by a corresponding decrease in medium and small aerosol fractions (Table 4, Figure 2). These patterns are clearly driven by the southern flank of the region (Figure 3), where there is *particular* enhancement in the very small aerosol fraction, SSA, oxidation, and normalized aerosol and CCN_{15} concentration compared to the northern flank. Particles in the southern flank are overwhelmingly very small and highly oxidized, and some reach SSA greater than 0.9. Note that the BBOP aircraft did not sample Region IV in the plume, as observed by MISR and MODIS (Figure 1).

II. Satellite Observations of the Government Flats Complex Fire

Table 5 quantifies the mean, standard deviation (SD or σ), and median values for the satellite observations for each region. The four subsequent sections provide qualitative analysis and context for these statistics, with an emphasis on *differences* between regions. It is important to reiterate that when discussing specific particle types (e.g., black carbon, brown carbon, dust, non-absorbing aerosols), the retrieved aerosol properties represent the optical equivalent of the aerosol present; i.e., the true aerosol can be a blend of the size, shape, spectral slope, and absorption of the retrieved components, and is not necessarily a mixture of the specific, retrieved components themselves.

Region I

The near-source region is strongly characterized by high REPA, with a mean SSA of 0.86 and a low SD indicating little variability (Figure 4). This can be attributed to: 1) a very large fraction of spectrally flat, BC-like components throughout the region, with a mean contribution of 56% to the total mid-visible AOD (and upwards of 90% in some pixels); 2) an almost zero AOD fraction of non-absorbing aerosols (mean ~10%, median nearly 0%); and 3) a significant AOD fraction of non-spherical aerosols (mean ~20%), which are weakly absorbing and represent "dust" analog (possibly soil) particles. There are also some pixels with noteworthy fractions of spectrally steep BrC-like aerosols, but their contribution in Region I (mean~13%, median<1%) pales in comparison to BC. Regional REPS is overall small, with a mean extinction Ångström exponent (ANG) of 1.54. However, REPS is more variable than SSA due to several lower-ANG pixels along the region's southwest edge, so the mean may overestimate true particle size (median ANG=1.58; Figures 4-5, Table 5). Component analysis indicates the REPS is the result of a mixture of very small and large aerosols, the latter likely primarily nonspherical particles (Figure S3).

Region II

The near-downwind region displays significantly lower REPA (mean SSA ~0.93), marked by a decrease in BC, BrC, and dust-analog fractions and an increase in non-absorbing component fractions (means ~36%, 8%, 11%, and 44%, respectively). REPS is also higher here than in Region I, although overall still considered small (mean ANG ~1.32). Geographic variability within the region can explain the large SDs in Table 5 – the central area is darker and dominated by BC and some dust-like particles similar to Region I, whereas the areas adjacent to the plume boundaries contain mostly non-absorbing particles, with essentially no non-spherical particles (Figures 4-5, Table 5). Furthermore, the southern portion of the region is retrieved as a mixture of large and very small aerosols, whereas the northern portion is dominated by medium and small aerosols (Figure S3).

Region III

The mid-downwind region displays REPA similar to Region II, although slightly darker overall, with a mean SSA of 0.92. However, there is significant geographic variability in the particle brightness between the northern vs. southern halves when the region is split lengthwise along the plume central axis. The SSA is much higher in the northeast than in the southwest. The entire region is distinct in that it is the only one to contain widespread, significant fractions of BrC-like components, based on the retrievals (regional mean ~30%, a 30-fold increase from upwind). This is accompanied by a corresponding overall regional decrease in the mean/median AOD fractions of the BC, dust, and non-absorbing particle analogs. However, the southern half of the region contains a BC fraction that appears at least equal to BrC. Furthermore, non-absorbing particles make a negligible contribution here, and there is a detectable fraction of the dust analog (~20-30%), all contributing to the low SSA overall. The northeast part of the region is dominated by both BrC and non-absorbing particles, whereas BC and dust fractions are nearly zero, which raises the SSA here. Despite the geographic variability in absorption, ANG is consistent throughout the region, with a mean of 1.82, the highest of all four regions (Figures 4-5, Table 5), indicating a predominance of smaller particles. Component analysis indicates both absolute and fractional increases in small aerosols (Figure S3).

Region IV

The far downwind region contains both the brightest and largest particles in the plume, with a mean SSA of ~0.97 and a mean ANG of ~1.04, so the region is still fine-mode dominated. The coverage in this region is not as extensive as in the other three, but one can still see somewhat coarse particles of ANG<0.7 along the plume edge, and somewhat finer-mode particles further upwind. Based on the retrievals, the region is largely dominated by non-spherical and non-absorbing components, the former being particularly evident at the plume edge. Both BC and BrC component fractions approach null (Figures 4-5, Table 5).

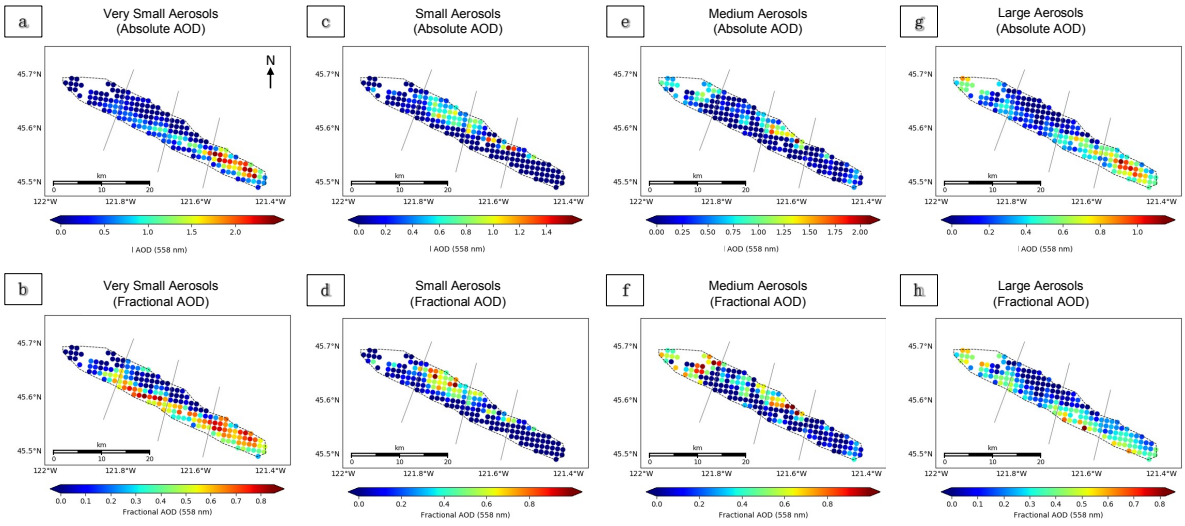

Figure S3. Absolute (top row) and fractional (bottom row) AOD of the four main particle size bins retrieved by the MISR RA for the Government Flats Complex Fire. Note: scales differ between categories.

Supplementary Material, Part 3

We present in the third part of this supplement detailed descriptions of the *in situ* and spacecraft observations collected for the Colockum Tarps Fire and the Douglas Complex Fire (briefly summarized in Section 3.4.1 and 3.4.2 of the main text). The aircraft and satellite observations of these fires were each separated by a day, which reduces their usefulness for formal validation of the satellite retrievals, but demonstrates the value in applying the satellite data in the vast number of situations where such data are available, but i*n situ* data are lacking.

I. Colockum Tarps Fire

The Colockum Tarps Fire, first ignited due to human causes, burned from July 25th, 2013 through August 15th, 2013 in southern central Washington. The primary fuel was a mixture of grass, brush, and timber; over 80,000 acres burned in total [59]. The July 26th, 2013 BBOP research flight and the subsequent July 27th MISR overpass observed the resulting smoke plume. Plume geometry changes significantly between observations; the plume extends toward the northeast from the fire source on July 26th, and toward the southeast on July 27th. The plume outline for the *in situ* observations was traced using the RGB MODIS Aqua image from ~20:10 UTC (Figure S4a; the aircraft flew in the area from ~20:00-22:20 UTC). There is a significant pocket of little-to-no smoke within the plume boundaries at this time, but as plume dynamics and smoke location may have changed during the course of the flight, we include this area within the boundary.

Measurements are considered "outside" the plume in areas where CO and aerosol concentrations were below thresholds of 0.11 ppm and 1000 #/cc, respectively, where measurements are particularly noisy, or where the plane was flying at an altitude thought to be above the smoke layer. These requirements usually all coincide (Figure S4c, d), and aircraft data obtained for points considered "outside" the plume, under very low particle concentration, are generally quite uncertain (e.g., the very low SSA values outside the plume boundaries in Figure S5a). Note also that the southern along-plume transect was flown at ~12:15 UTC, the very beginning of the ~2.5-h sampling period. As such, the seemingly anomalous along-plume data between cross-plume transects 3 and 4 in Figures S5 a, b, and c was probably outside the plume boundary at acquisition time, unlike the geographically nearby cross-plume transects obtained an hour or more later. The following day, as shown in the broader-swath MODIS imagery (Figure S4b), MISR sees some, but not all, of the visible plume extent.

Aircraft Observations of the Colockum Tarps Fire

The flight observations depict a plume with particle properties that appear to change less systematically with downwind distance than the Government Flats Complex Fire, making it difficult to divide the plume neatly into characteristic regions as was done in Section 3 of the main text. From the measured wind speeds, we estimate the visible plume age to be ~226 minutes (~3.8 h) along the cross-plume transect indicated by the line in Figure S4a at the time of the flight.

Particle properties vary on short spatial scales (~1 km); however, some larger-scale patterns are also evident. There is an area of optically very thick smoke in the apparent source region(s), characterized by high total aerosol count, oxidation state, SSA, CCN concentration, and BC fraction and concentration, relative to background over most of the plume extent (Figures S4 and S5). However, very near the source, the particles are highly light-absorbing, with oxidation values near zero and SSA of 0.75 or lower – these SSA values are expected to be biased low due to measurement bias with the PSAP. In general, the plume is dominated by "small" particles, with "very small" particles contributing second-most, based on particle counts, and moderate contributions from medium aerosols in some areas (Figure S6). Large particles are essentially absent, with fractional contributions well below 1%. When split lengthwise along the plume's

central axis, the plume displays somewhat larger particle size toward the northern edge, where medium aerosols contribute up to 20% of the total aerosol count. The fraction of small aerosols is also somewhat higher here, whereas very small particles make up a noticeably smaller fraction. From plume source to nominal end, particle size overall appears to increase slightly along the plume central axis, to the extent this is sampled by the aircraft.

As mentioned above, particles sampled along the cross-plume aircraft transect closest to the source are highly absorbing and very fresh (Figures S5a and S5b). Both CCN number and BC mass concentrations also peak near the source, as might be expected. BC and CCN concentrations decrease considerably downwind within the near-source region, and oxidation state increases. There is also an increase in the CO-normalized aerosol concentration between the first two near-source, cross-plume aircraft transects (Figure S5f), indicating possible new particle formation shortly after emission, but there is no evidence in these data for additional particle production further downwind, and the increased concentration could arise from wind-driven convergence or changing emission at the source. Downwind of the first, near-source transect, SSA increases gradually over the length of the plume, BC and CCN concentrations remain relatively constant, whereas oxidation state and normalized CCN concentration are more variable. Toward the plume end (~226 minutes of aging), particles are only moderately absorbing (SSA ~0.9), are oxidized substantially ($-\log[NO_x/NO_y] > 0.6$) and contain considerably less BC mass contributing to the overall aerosol mass loading. The gradual increase in SSA downwind, despite relatively constant BC fraction, could be due to particle hydration, as the small-particle fraction increases relative to the very small particle fraction. It could also be due to the condensation of VOC's onto existing aerosols, leading to increasing particle diameter of OA and increased coating thickness of BC-containing particles. Most BC-containing particles are less than 0.1 μm in radius, with smaller sizes of ~0.06 μm closest to the source and larger particles, ranging from 0.07 up to 0.1 μm, downwind. Overall, $r_{e(BC)}$ does not follow any systematic spatial pattern in the available data (Figure S7).

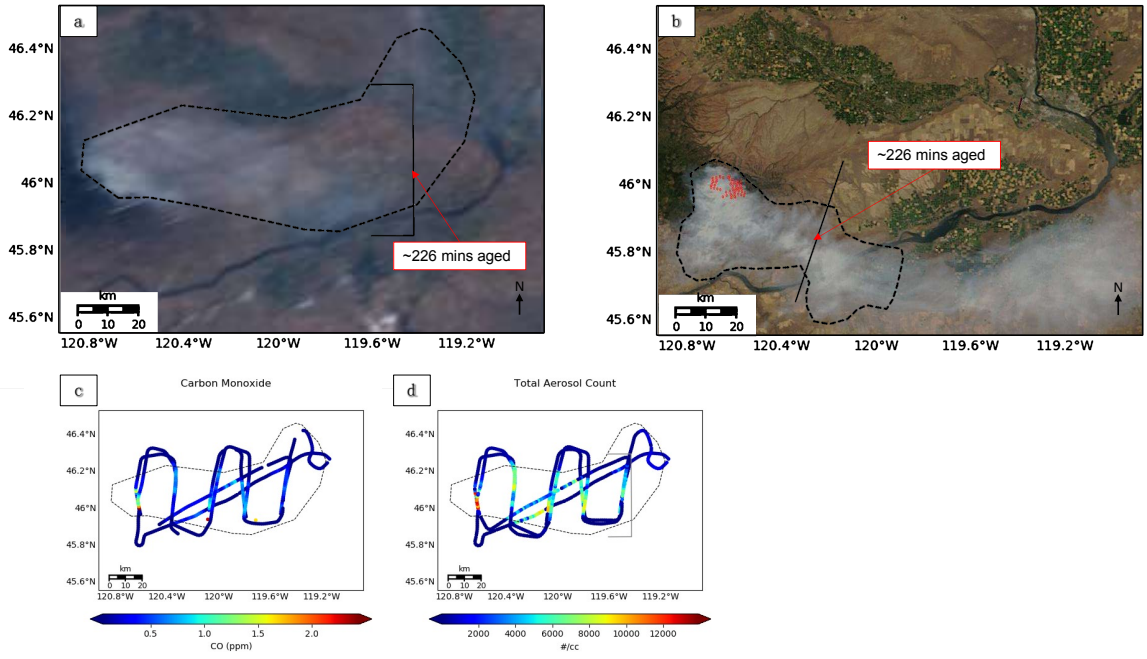

Figure S4. The Colockum Tarps fire in southern central WA as seen: **(a)** during BBOP flight operations, ~20:00-22:20 UTC on July 26th, (20:10 UTC, MODIS Aqua RGB image), and **(b)** at MISR overpass time on July 27th (19:13 UTC, MODIS Terra RGB image). The red dots indicate MODIS-identified hot spots and are used to estimate source location. The near-source plumes are outlined with thin dashed lines in these figures, and the

location of smoke within the plume estimated as having aged ~3.8 hours is marked with a thin solid line. Panels **(c)** and **(d)** are maps of the aircraft *in situ* CO and total aerosol count measurements on July 26th, respectively.

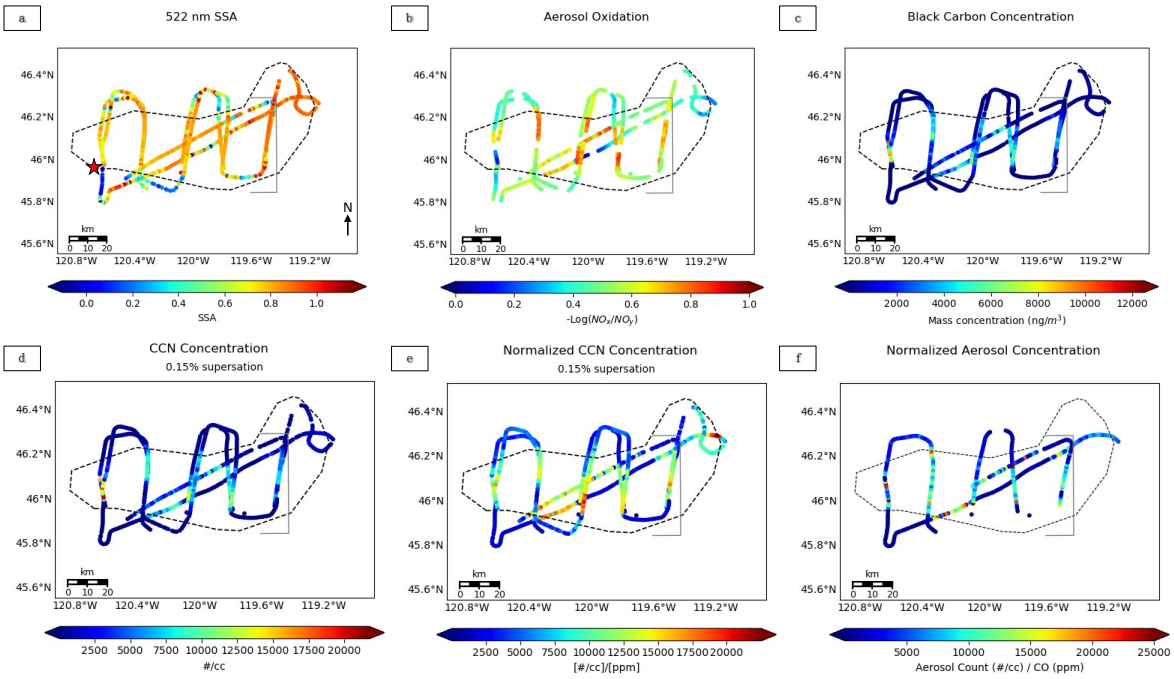

Figure S5. Aircraft observations from the Colockum Tarps fire in southern central WA of **(a)** 522-nm SSA (PSAP/neph), **(b)** aerosol oxidation (derived from 3-channel Oxides of Nitrogen Analyzer), **(c)** Mass concentration of BC and size of BC-containing particles (SP2), **(d)** the concentration of particles that can act as CCN at 0.15% supersaturation (CCN-200 instrument), **(e)** the CCN concentration divided by the CO concentration, and **(f)** the total aerosol concentration divided by the CO concentration. The star in (a) serves a reminder of the source location.

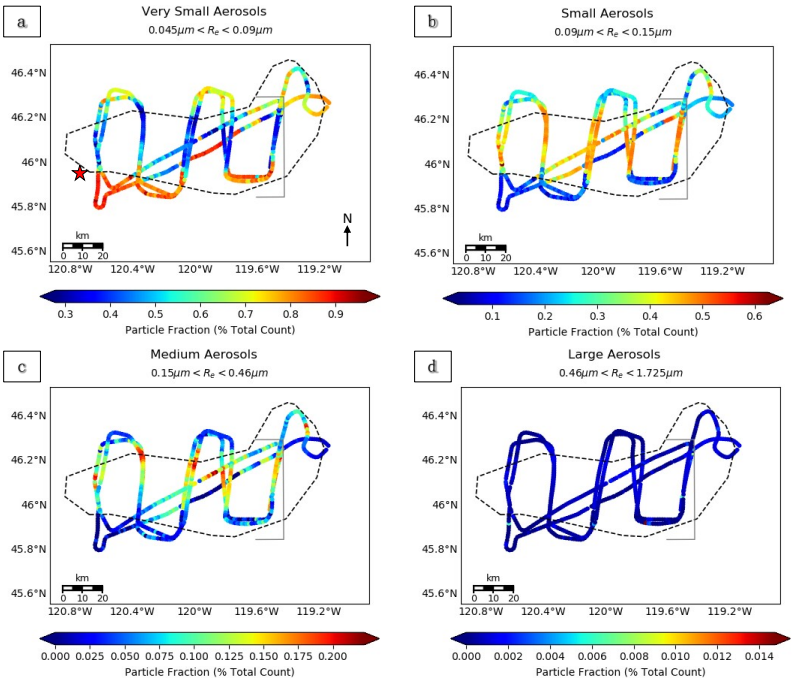

Figure S6. Fractional contributions to the total aerosol count for very small **(a)**, small **(b)**, medium **(c)**, and large **(d)** aerosols in the Colockum Tarps fire in southern central WA, as measured by the PCASP and CAS *in situ* instruments. The star in (a) serves a reminder of the source location. Note: scales differ between categories.

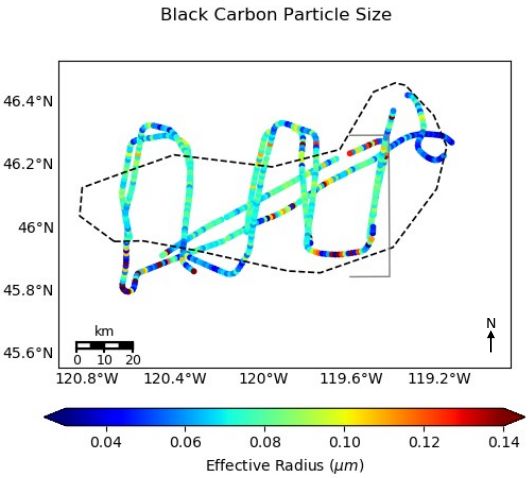

Figure S7. $r_{e(BC)}$ for the Colockum Tarps fire observed by the SP2 aboard the BBOP G-1 aircraft.

MISR Observations and Discussion for the Colockum Tarps Fire

The next-day satellite observations show significant changes in plume geometry. The plume boundaries are better defined on this day (Figure S4), and the satellite retrievals provide significant context beyond the aircraft transect observations. MISR-MINX stereo heights indicate the smoke stays mostly below 4 km and has a median height of ~2.9 km ASL (Figure S8a-b). Approximately 40 km downwind, the smoke becomes lofted about 1 km higher than the upwind area. At around this distance, the plume age is ~226 minutes (~3.8 h), as estimated from wind speed roughly along the plume axis, at plume elevation

(Figure S8c). The smoke is also optically very thick, with a nominal-retrieved mid-visible AOD near the source of 9, though the uncertainty in retrieved AOD becomes large once AOD exceeds a value of 4 or 5. The extinction Ångström exponent (ANG) suggests the plume at this time is dominated by small-to-very-small particles overall (median ANG ~1.74), particularly near the source (Figure S8e). Component analysis suggests heavy weighting of very small aerosols near the source, and a mixture of mostly small but also some medium particles downwind, with a near-complete lack of larger particles, as on the previous day (Figure S9).

As expected, the particles are darkest near the source. There is a patch of very small, dark particles extending from the source to about 20 km downwind along the northern boundary of the plume, with SSA ~0.83 or lower and ANG ~3.0 or higher. However, the particles brighten downwind and to the south, with SSA above 0.97 in some places (median plume SSA ~0.90) (Figure S8f). The SSA values and their observed increase with age is consistent with that reported by *Sedlacek et al*. [19]. Further analysis of the RA components suggests that particles near the source are primarily a mixture of BC- and BrC-like aerosols, with some nonabsorbing particles, but that BrC is confined near the source so that the downwind region is retrieved entirely as BC and non-absorbing aerosols (Figure S10), yielding a net mid-visible SSA ~0.93. The apparent, abrupt particle-type transition might indicate changes in the burning conditions at the fire rather than particle evolution after emission.

Taken together, the satellite and *in situ* observations describe a plume with fine-mode, highly absorbing particles near the source that become brighter downwind. The MISR RA differs from the aircraft measurements in that it derives mostly very small particles near the source, with a significant increase in particle size a short distance downwind, whereas the aircraft CAS and PCASP observe particles *in situ* that are mostly in the same small size category throughout the plume (with pockets of enhanced medium particle fractions, similar to the pockets of lower ANG in the MISR RA). The difference in initial particle size could reflect changes in smoke properties between the two days or could be due to *in situ* measurement selective sampling, whereby plume properties would be more completely represented when the entire region is mapped with satellite observations.

The upper ranges of observed SSA values between the two days are very similar; in both cases, highly scattering aerosols, having SSA above 0.95, appear far from the source. As mentioned in the discussion of the Government Flats Complex Fire, the fact that the RA does not observe SSA as low as the aircraft could be due to the finer spatial resolution at which the aircraft samples, the limitations of filter-based measurements, or to limitations in the RA particle climatology. Regardless, the same general light-absorption patterns apparently persist day to day for the Colockum Tarps Fire. A more noticeable difference is that BC mass concentration peaks near the source and decreases threefold after the first cross-plume transect, and then appears relatively constant further downwind during aircraft operations on July 26th (Figure S5c), whereas on July 27th, the MISR RA indicates that BC AOD varies but preserves high values in patches over much of the plume downwind (Figure S10a-b). This difference could also be explained by limited aircraft sampling, though changing fire emissions cannot be ruled out.

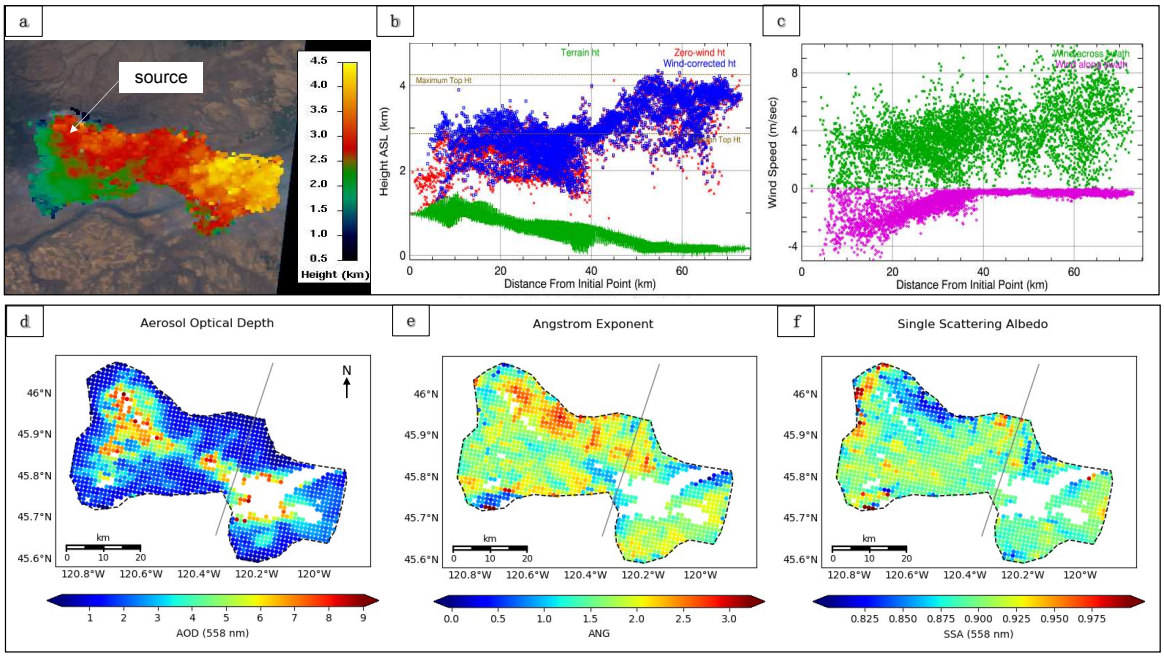

Figure S8. Plume properties for the Colockum Tarps fire in southern central WA retrieved by MISR at 19:13 UTC (Orbit 72382, Path 46, Blocks 53-54). **(a)** MISR-MINX stereo height retrieval map, **(b)** MINX stereo height profile as a function of distance from the source, for both zero-wind (red) and wind-corrected (blue) analyses, with surface elevation indicated in green, **(c)** the MINX-derived across-swath and along-swath wind vectors at plume level, **(d)** the RA-derived AOD at 558 nm, **(e)** ANG, and **(f)** the SSA at 558 nm. The transect for plume age estimated at ~226 minutes is indicated with a thin gray line in panels d-f.

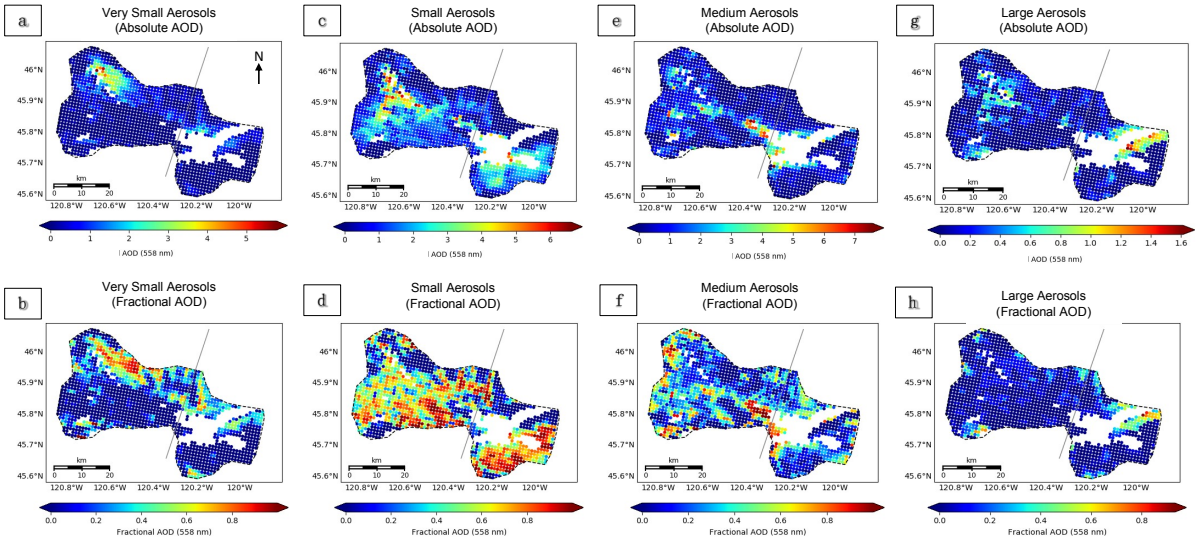

Figure S9. Absolute (top row) and fractional (bottom row) AOD of the four main particle size bins retrieved by the MISR RA for the Colockum Tarps fire. Note: scales differ between categories.

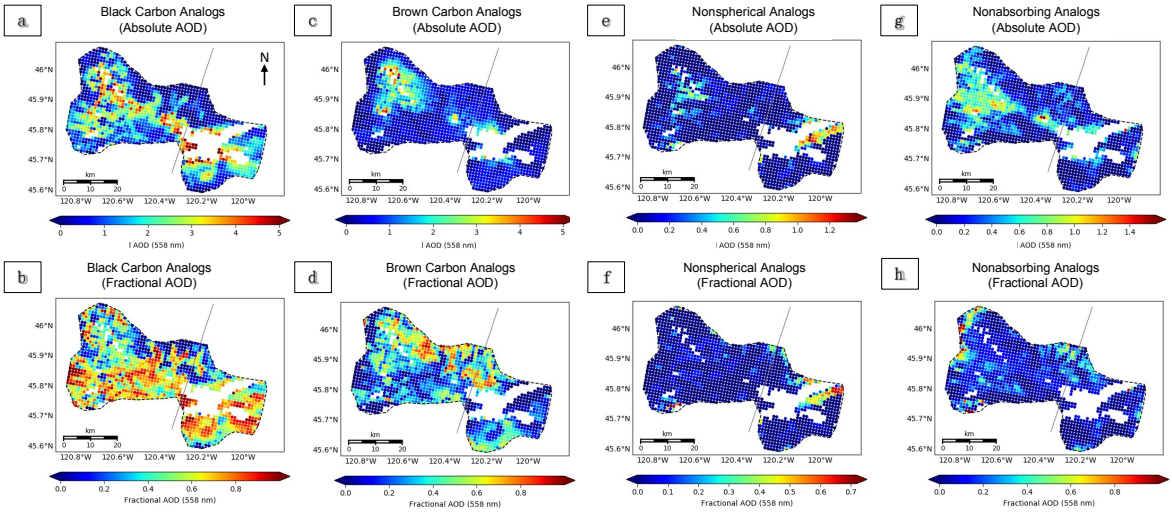

Figure S10. The absolute and fractional AOD of various MISR components, for the Colockum Tarps fire in southern central WA, where **(a-b)** are the sum of all "flat," i.e., BC-like components, **(c-d)** are the sum of all "flat," i.e. BrC-like components, **(e-f)** are the non-spherical dust-like component, and **(g-h)** are the sum of all non-absorbing components.

II. Douglas Complex Fire: Satellite Observations Preceding Aircraft Observations

The Douglas Complex fire was a large system originally comprised of dozens of lightning-sparked fires that ignited on July 26th, 2013 and burned through August 19th, 2013 in southern coastal Oregon. The fuel was a mixture of old growth and second growth conifer [58]. The August 5th, 2013 MISR overpass and the subsequent August 6th BBOP research flight observed the smoke plumes that were produced (Figure S11). The outline for the *in situ* observations was traced from the MODIS-Terra RGB image at 19:51 UTC (flight operations took place in the area from approximately 19:30-21:00 UTC). As one can see in Figure S11b, the plume outline selected does not fully capture all of the smoke in the scene; it is just meant to provide a reference for the apparent core region of the plume.

MISR Observations of the Douglas Complex Fire

On August 5th the plume had a well-defined plume core (Figure S11a), with AOD exceeding the nominal MISR RA AOD upper limit of 9 (Figure S12d), with a large uncertainty. The plume does not rise above 2.0 km ASL, and median smoke height is ~1.17 km ASL, which is not much above the terrain in this topographically complex region (Figure S12b). Wind speeds are low throughout the observed area (Figure S12c), which might explain the difficulty in locating the plume source, as the smoke tended to pile up over a small area. MISR-retrieved particle size and light-absorption data indicate the plume core is dominated by small-medium, moderately absorbing aerosols (ANG≤1, SSA~0.87-0.92), whereas the surrounding, lower-AOD areas contain smaller, weakly or nonabsorbing particles (ANG>1, SSA~0.92-1.0) (Fig. S12e, S12f). Component analysis reflects the larger REPS and lower REPA in the plume core than the surroundings (Figures S12 and S13). Spectrally steep BrC and non-spherical dust optical analogs are also retrieved, concentrated in the core (Figure S14c-d and e-f, respectively). The retrieved non-spherical component suggests there may be externally mixed dust or soil particles ejected into the atmosphere during intense burning, or a lack of spherical particles of similar size distribution and SSA to the dust analog in the algorithm climatology (Table 2).

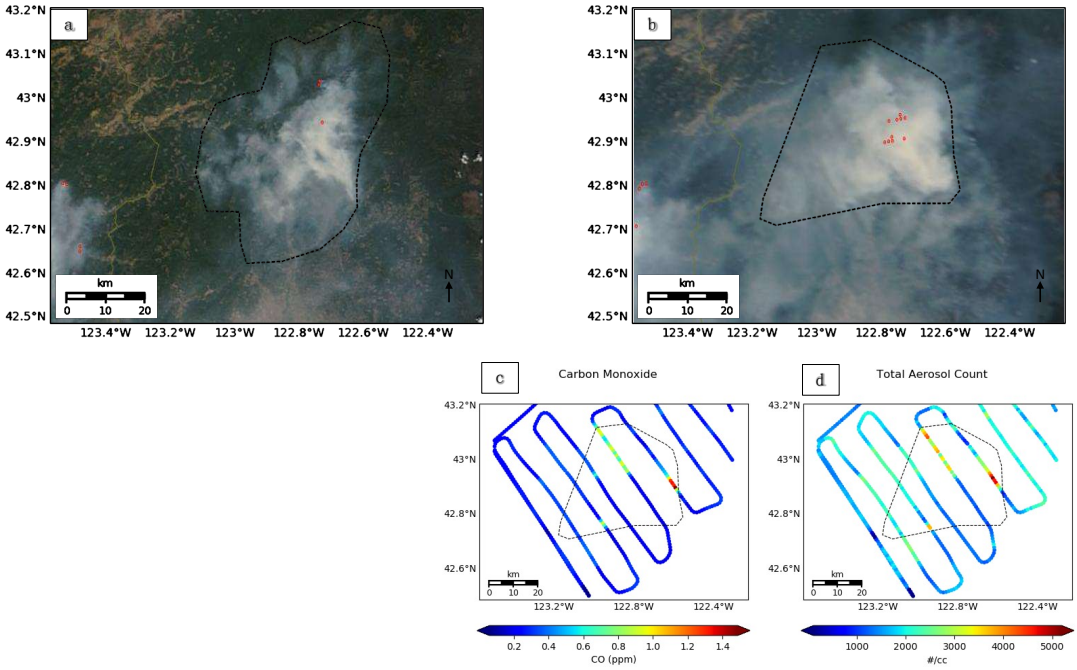

Figure S11. The Douglas Complex fire in southern coastal OR as seen: **(a)** at MISR overpass time on August 5th (19:08 UTC; MODIS Terra RGB image), and **(b)** during BBOP flight operations ~19:30-21:00 UTC on August 6th (19:51 UTC; MODIS Terra RGB image). The red dots indicate MODIS-identified hot spots, and are used to estimate source location. Panels **(c)** and **(d)** are maps of the aircraft CO and Total Aerosol Amount on August 5th, respectively.

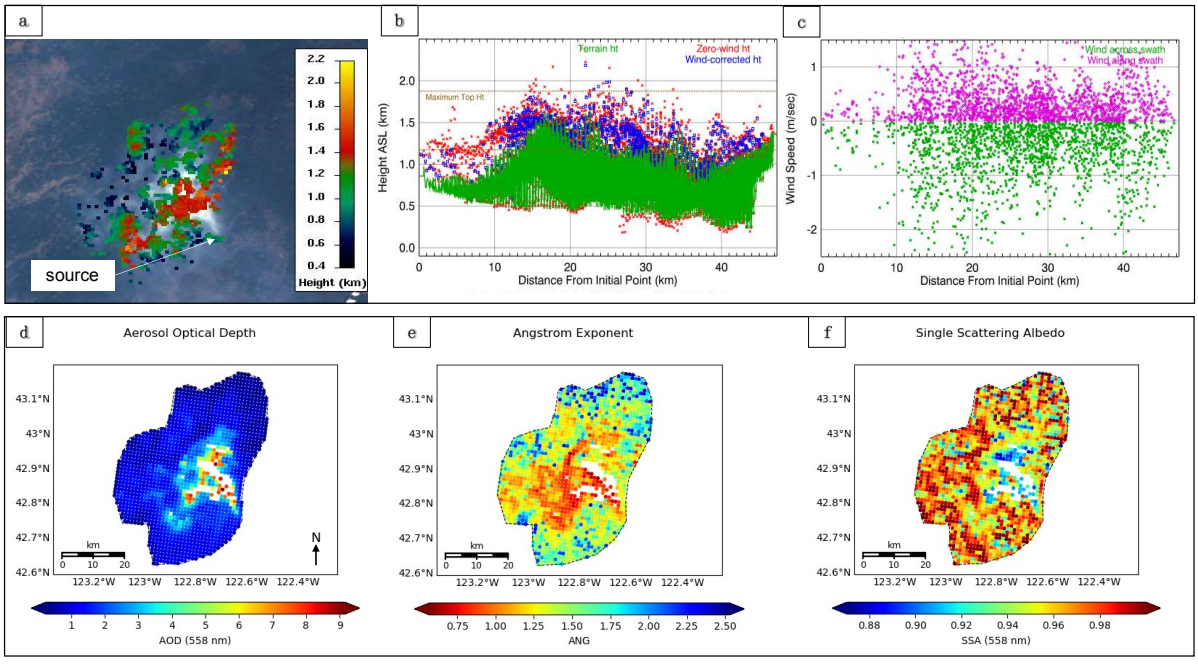

Figure S12. Plume properties for the Douglas Complex fire in southern coastal OR retrieved by MISR at 19:08 UTC (Orbit 72513, Path 45, Block 56). **(a)** MISR-MINX stereo height retrieval map, **(b)** MINX stereo height profile as a function of distance from the source, for both zero-wind (red) and wind-corrected (blue) analyses,

(c) the across-swath and along-swath wind vectors, **(d)** the RA-derived AOD at 558 nm, **(e)** ANG, and **(f)** the SSA at 558 nm.

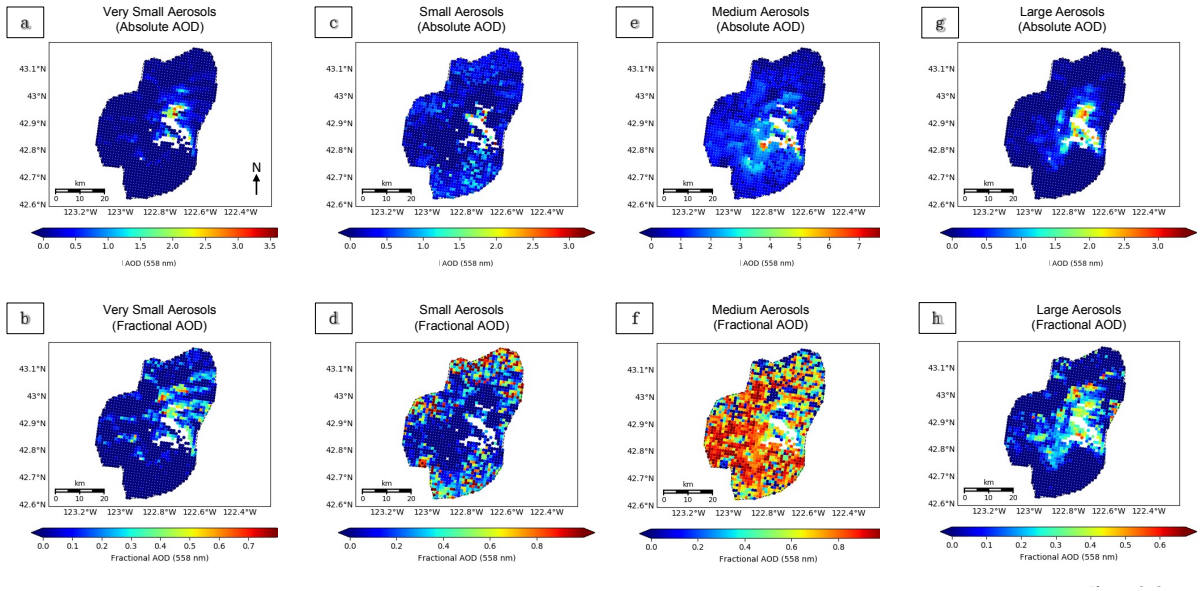

Figure S13. Absolute (top row) and fractional (bottom row) AOD of the four main particle size bins retrieved by MISR for the Douglas Complex fire. Note: scales differ between categories.

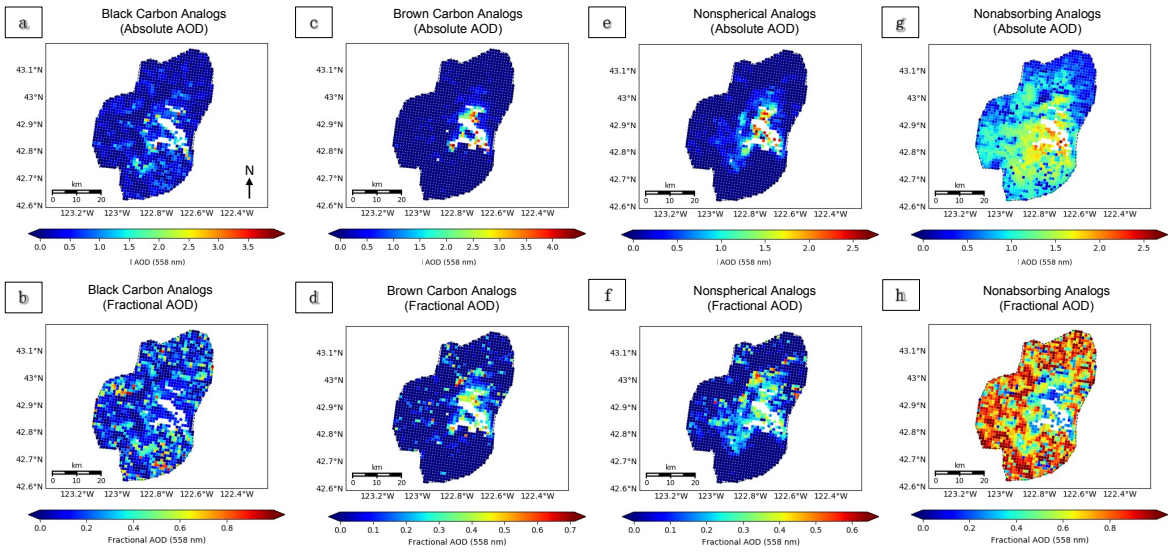

Figure S14. The absolute and fractional AOD of various MISR components for the Douglas Complex fire in southern coastal OR, where **(a-b)** are the sum of all "flat," i.e. BC-like components, **(c-d)** are the sum of all "flat," i.e. BrC-like components, **(e-f)** are the non-spherical dust-like component, and **(g-h)** are the sum of all non-absorbing components.

Aircraft Observations and Discussion for the Douglas Complex Fire

The BBOP *in situ* plume observations on the following day describe a scene with an expanded plume core area and considerable, diffuse smoke in the immediate surroundings (Figure S11b). The maximum CO and aerosol concentrations in the available measurements are located near the MODIS-identified hot spots (Figure S11c-d), but the aircraft did not fly directly over these spots, so the actual distribution is ambiguous. The sampled near-source areas also contained some of the brightest and the most highly oxidized particles in the available data record (Fig. S15a, b). However, they also contain the most BC mass of this plume (Figure S15c), though much less than the sampled regions of the Government Flats and July 26th Colockum Tarps fire plumes. (This could be a consequence of the elevation at which the aircraft sampled rather than the peak smoke concentrations of the Douglas Complex fire.) The particles in the plume core are primarily small and medium in size, whereas the particles in the surroundings are mostly very small and small (Figure S16). BC effective particle size ($r_{e(BC)}$) shows no distinct pattern over the aircraft-sampled region (Fig. S17).

The combined information from the satellite and the aircraft data suggest larger particle sizes in the thickest parts of the plume compared to the surroundings. These particles fall within the small to medium size range; however, the RA retrieves overall slightly larger particles than the aircraft data on the previous day, including a significant contribution from large particles in the plume core. Particles near the source are moderately light-absorbing as seen by MISR (SSA ~0.92) but are brighter the next day during flight operations (SSA ~0.95), when the fire appears to be a bit more active in the imagery (Figure S11).

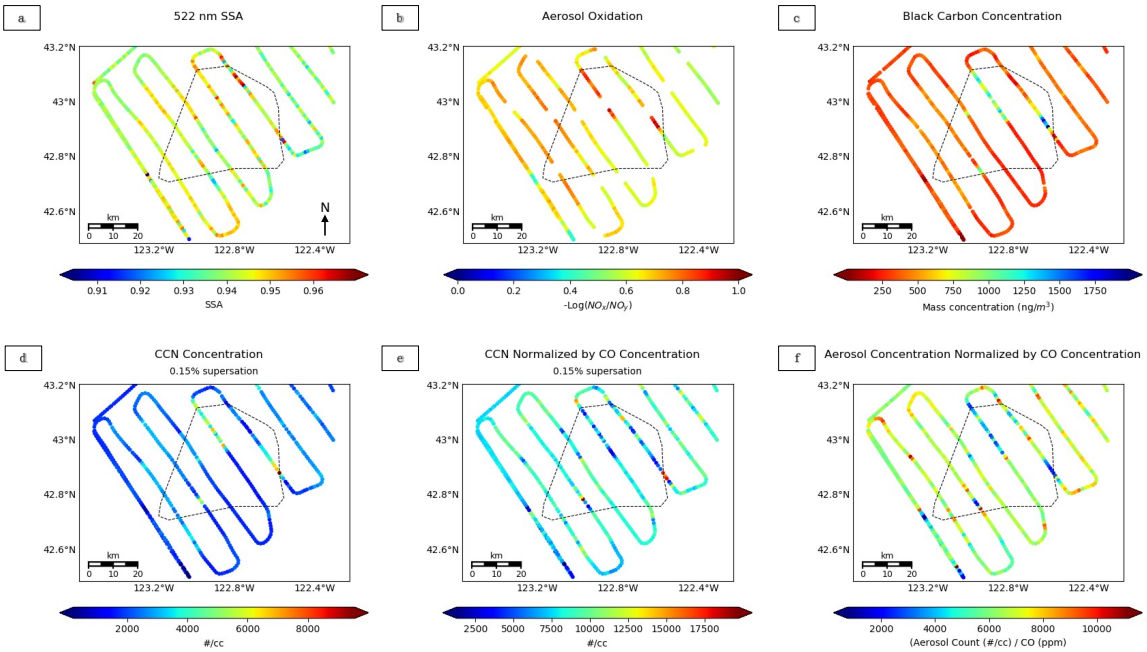

Figure S15. Aircraft observations from the Douglas Complex fire in southern coastal OR of **(a)** 522-nm SSA (PSAP/neph), **(b)** aerosol oxidation (derived from 3-channel Oxides of Nitrogen Analyzer), **(c)** Mass concentration of BC and size of BC-containing particles (SP2), **(d)** the concentration of particles that can act as CCN at 0.15% supersaturation (CCN-200 instrument), **(e)** the CCN concentration divided by the CO concentration, and **(f)** the total aerosol concentration divided by the CO concentration.

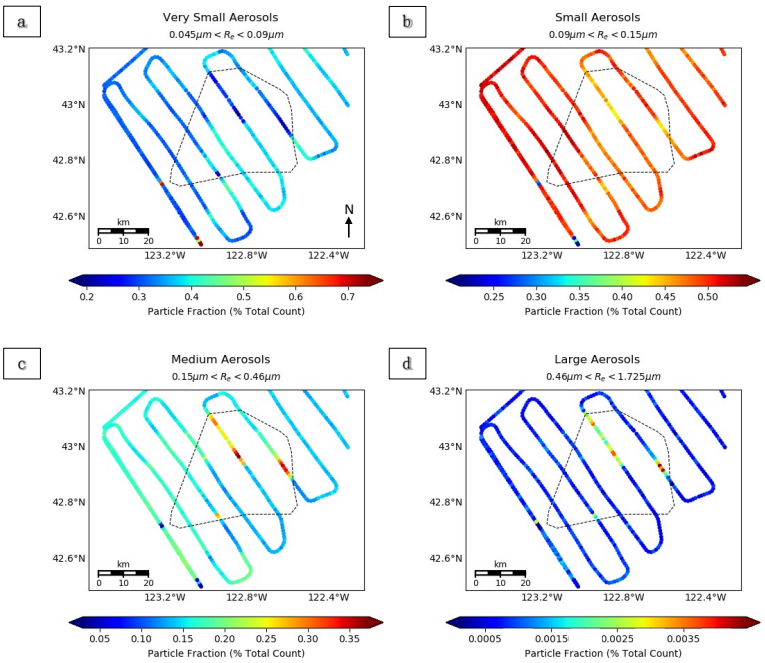

Figure S16. Fractional contributions (from zero to one) to the total aerosol count for very small **(a)**, small **(b)**, medium **(c)**, and large **(d)** aerosols in the Douglas Complex fire in southern coastal OR, as measured by the PCASP and CAS *in situ* instruments. Note: scales differ between categories.

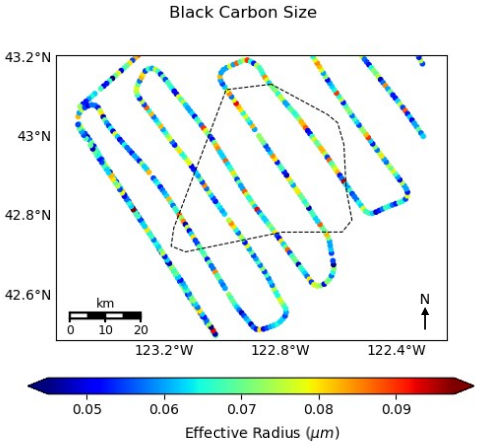

Figure S17. $r_{e(BC)}$ for the Douglas Complex fire, observed by the SP2 aboard the BBOP G-1 aircraft.